Anal. Bioanal. Electrochem., Vol. 14, No. 10, 2022, 968-979

Analytical & Bioanalytical Electrochemistry

www.abechem.com

Full Paper

High Performance of $NiMn_2O_4$ Nanostructured Electrode for Supercapacitor Applications

M. Puratchimani,[1] V. Venkatachalam,[2,*] M. Rajapriya,[3] and K. Thamizharasan[2]

[1]*Department of Physics, As-Salam College of Engineering and Technology, Thirumangalakudi, Aduthurai-612 012, India*

[2]*Department of Physics, Sir Theagaraya College, Chennai-600 021, India*

[3]*Department of Chemical Engineering, SSN College of Engineering, Chennai-600 123, India*

*Corresponding Author, Tel.: +91-9444014282

E-Mail: venkatcnst12@gmail.com

Received: 15 July 2022 / Received in revised form: 18 October 2022 / Accepted: 19 October 2022 / Published online: 31 October 2022

Abstract- In this present work, $NiMn_2O_4$ nanostructures were prepared by using KOH/NaOH double hydroxide solution by hydrothermal method. The structure and chemical composition of the prepared material was confirmed by XRD and FT-IR, respectively. HR-TEM revealed the surface morphology of the $NiMn_2O_4$. The enhanced electrochemical properties of the $NiMn_2O_4$ material were examined by the CV, CP, and EIS analyses. The supercapacitor based on the nanostructured $NiMn_2O_4$ revealed the higher specific capacitance (854.7 F/g at 5mV/s in 2 M aqueous KOH electrolyte), better performance and cyclic stability (94.6% capacitive retention after 1000 cycles at 4 A/g). The hexagonal morphology plays an important role in enhancing the specific capacitance of the electrode. The electrochemical behaviors infer that the hexagonal-like $NiMn_2O_4$ nanostructured electrode can be potentially used in supercapacitors.

Keywords- $NiMn_2O_4$; Cubic-like structure; Electrochemical properties; Double hydroxide medium

1. INTRODUCTION

In recent years, supercapacitors (SCs) have widespread interest because of their worldwide electronic industry applications such as memory backup systzef0em, pacemakers, energy management, portable electronic gadgets and electronic vehicles, due to their high thermal stability, low cost, fast charge-discharge rates, high power density, good reversibility and long cycle life [1-4]. Depending on the charge storage mechanism, supercapacitors can be classified into two types: (i) electrochemical double layer capacitors (EDLCs) and pseudocapacitor (PCs). In particular, the energy densities and capacitance of PCs are two orders of magnitude higher than EDLC. Therefore, various kinds of pseudocapacitive materials such as Co_3O_4, NiO and MnO_2 have been studied which exhibited good electrochemical performance owing to their ultrahigh theoretical specific capacitances and different states of oxidation for redox reactions [6,7]. However, there are some drawbacks for transition metal oxides such as short cyclic lifetime and low electronic conductivity.

Researchers have recently found that binary transition metal oxides have improved electrochemical properties than the metal oxides due to their higher electronic conductivity and different oxidation states. Mixed transition metal oxides (MTMOs), formation a binary or ternary transition metal oxides have been shown aiding the charge transportation towards current collector, better improved charge transfer process at the electrode-electrolyte interface and electrochemical properties of the electrode [8]. Hence, binary transition metal oxides are found to be a next-generation high-performance and promising electrode materials for energy storage device applications.

Binary transition metal oxides with various nanostructures such as, $NiCo_2O_4$, $CoFe_2O_4$, $FeCo_2O_4$, and $NiMn_2O_4$ have been utilized and considered to be a potential material for high - performance supercapacitor [9-12]. Among different structures of binary metal oxides, AB_2O_4 based spinel structured materials have great interests owing to their outstanding physico-chemical properties. Furthermore, the Mn-based binary transition metal oxides have also been studied for supercapacitors. Particularly, the spinel structured $NiMn_2O_4$ electrode material has great research attention because of its non-toxic ternary metal oxide, high conductivity and redox active sites, low cost, stability, better structural stability, higher capacitance and the multiple valences of Mn oxides and high electrochemical activity of Ni oxides for potential applications such as catalysis [13], and sensors [14], compared with single Mn-based oxides. The $NiMn_2O_4$ electro-active materials were prepared by various methods such as sol-gel, co-precipitation and hydrothermal method. Among them, hydrothermal technique is one of the best methods and it provides the simplicity coupled with a relatively one-step synthesis process, effective route to control the size and shape, environmentally friendly and low-cost operational process. However, there are relatively few works about $NiMn_2O_4$. For example, H.M. Lee et al. reported the manganese–nickel oxide films with the specific capacitance of 424 Fg^{-1} in Na_2SO_4 electrolyte [15]. M.Y. Arsent'ev et al. reported spinel $NiMn_2O_4$ material with the high

specific capacitance of 184 F/g in 1M $LiNO_3$ [16]. However, the improvement of the electrochemical properties of $NiMn_2O_4$ can be attained by low-cost preparation process for superior performance.

In this present work, $NiMn_2O_4$ nanostructured material synthesized through equal mole ratio of double hydroxide medium involving potassium and/ sodium hydroxide solution through a simple hydrothermal technique. The electrochemical properties were studied by using cyclic voltammetry (CV), chronopotentiometry (CP), long cycle stability and electrochemical impedance spectroscopy (EIS) in 2 M KOH aqueous electrolytes. Interestingly, $NiMn_2O_4$ electrode has showed the highest specific capacitance of 854.7 F/g at 1 A/g in 2 M KOH aqueous electrolyte with 94.6% capacitive retention. The $NiMn_2O_4$ nanostructure revealed the improved electrochemical behaviors with long cycle stability and can be a promising material for high performance energy storage device applications in supercapacitor.

2. MATERIALS SYNTHESIS

2.1. Materials

Sodium hydroxide (NaOH, MERCK), potassium hydroxide (KOH, MERCK), Zinc Nitrate **(**$ZnNO_3$, MERCK), and manganese Nitrate ($MnNO_3$, MERCK). All chemicals were purchased and used without any further purification. Throughout the reaction, an aqueous electrolyte was prepared by using laboratory-prepared double distilled water.

2.2. Material Synthesis

Double-hydroxide mediated synthesis of $NiMn_2O_4$ nanostructure is described as follows: initially, a 1:2 molar ratio of Nickel nitrate ($Ni(NO_3)$) and Manganese nitrate ($Mn(NO_3)$) solution was prepared in a beaker containing 40 ml of doubled distilled water by stirring. Subsequently, 9g of mixed hydroxides (equal molar ratio of KOH and NaOH pellets) was dissolved in 40 ml double distilled water and added to the above solution. Then, to ensure homogeneity, the two solutions were thoroughly mixed for a few minutes by stirring. After that, the above solution was shifted into the Teflon line autoclave and placed in a furnace for 24 h at 180 °C. The autoclave was cooled down naturally to room temperature after the completion of the reaction. The final precipitate product was obtained by washing and filtering with de-ionized (DI) water and then ethanol was used several times to remove the impurities by using centrifugation. After calcination at 400ºC for 4 hr, the product was collected for further characterization.

The possible chemical reaction can be expressed for $NiMn_2O_4$ material as given below,

$$Ni^{2+} + 2OH^- \rightarrow Ni(OH)_2 \quad (1)$$

$$Mn^{2+} + 2OH^- \rightarrow Mn(OH)_2 \quad (2)$$

$$2Mn(OH)_2 + Ni(OH)_2 + 1/2\ O_2 \rightarrow NiMn_2O_4 + 3H_2 \quad (3)$$

These results revealed in the formation of pure $NiMn_2O_4$ nanostructures.

2.3. Characterization

The crystal structure of the $NiMn_2O_4$ material was examined by powder X-ray diffraction (XRD, Rigaku mini flux (II)-c). By using the Debye-Scherrer formula, the average crystallite size of the material was evaluated by:

$$d = \frac{0.9\times\lambda}{\beta\times cos\theta} \quad (1)$$

where λ-is the x-ray wavelength, β– is the full-width half-maximum, θ –is the Bragg diffraction angle, and d- is the crystallite size. The FT-IR (Perkin Elmer spectrometer with KBr pellet) analysis was obtained in the frequency range from 4000 to 400 cm^{-1}. The morphology of the prepared sample was visualized through High-resolution transmission electron microscopy (HR-TEM, Hitachi H7650).

2.4. Electrochemical analyses and electrode preparation

The working electrode was prepared as follows; in the weight ratio of 8:1:1, the $NiMn_2O_4$ material was mixed with PVDF (polyvinylidene difluoride) and activated carbon. To get the homogeneity of the above mixture one drop of 1-methyl-2-pyrrolidinone was added and then, the mixed material was coated onto a nickel foil (NF). Electrochemical studies were analyzed by using the three-electrode system employing with Ag/AgCl as the reference electrode, NF as the working electrode and the platinum wire as the counter electrode in electrochemical workstation (Bio-logic VMP3, France). The electrochemical performances of the $NiMn_2O_4$ electrode were evaluated by CV within a potential window between 0.0 and 0.8V at various applied scan rates from 5 to 100 mV/s. The CP characteristics were observed at applied different constant current from 0.0 to 0.6V. EIS analysis was also carried out in the frequency region between 1Hz and 1MHz. Through CV and CP techniques, the specific capacitances of the $NiMn_2O_4$ electrode were evaluated.

3. RESULTS AND DISCUSSION

3.1. XRD analysis

The XRD pattern of the $NiMn_2O_4$ nanostructures as shown Figure 1. All the observed peaks are well indexed with $NiMn_2O_4$ face centered cubic phase (JCPDS no. 71-0852), which are found to be well matched with early reports [17]. All the diffraction peaks are consistent with the standard spinel structure of $NiMn_2O_4$ with space group Fd-3m. The broad XRD peaks are owing to smaller grain size of the nanostructures. There are no other peaks were observed

in the diffraction pattern, which confirms the phase purity and complete transformation of the Ni – Mn precursors into $NiMn_2O_4$ spinel structure.

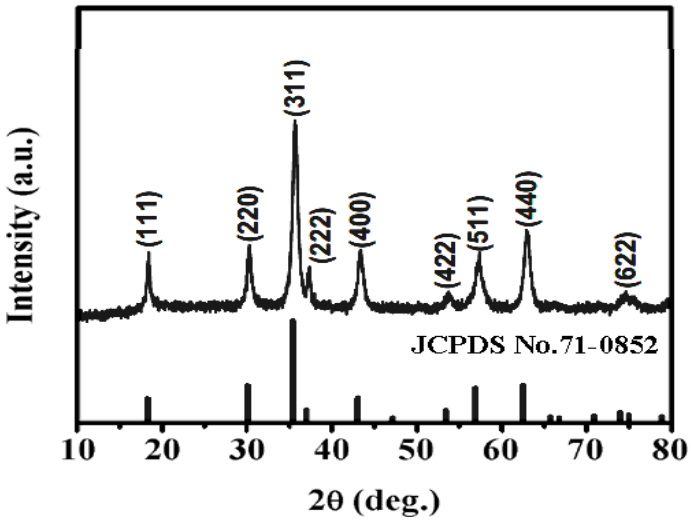

Figure 1. XRD pattern of the $NiMn_2O_4$ nanostructures

3.2. FT-IR studies

Figure 2 shows the FT-IR spectrum of the $NiMn_2O_4$ nanostructures was recorded in the frequency range from 400 to 4000 cm^{-1}. The two main characteristic bands were obtained at 426.4 and 532.6 cm^{-1} due to the octahedral Ni^{2+}–O^{2-} and tetrahedral Mn^{3+}–O^{2-} vibrational modes which further confirms their single-phase spinel $NiMn_2O_4$ structure. The stretching vibration of CO_2 coming from the atmosphere was observed at 1590.6 cm^{-1}.

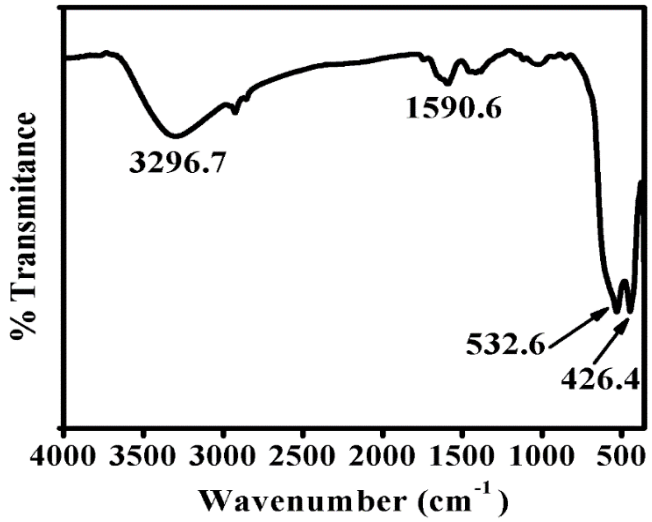

Figure 2. FT-IR spectrum of the $NiMn_2O_4$ nanostructures

The stretching vibration of O-H group due to H_2O molecules physio-adsorbed on the surface of the material was appeared at 3296.7 cm^{-1}. Such surface-adsorbed H_2O molecules

improve the wettability of the electrode, which would enhance the electrochemical behavior of the material [18]. Finally, the lower frequency region absorption bands are suggesting the formation of spinel $NiMn_2O_4$ nanostructure.

3.3. Morphology analysis

The HR-TEM images of the $NiMn_2O_4$ material are shown in Figure 3. Further, the nanostructures of the resulting powders were characterized using HR-TEM, as shown in Figure 3(a,b). The HR-TEM images revealed the interconnected, disordered cubic-like, and homogeneously distributed nanostructure. The formation of such disordered cubic-like $NiMn_2O_4$ nanostructures can effectively generate active sites during the electrochemical reactions, which enhances the electrochemical properties of the electrode. The SAED pattern, shown in Figure 3(c) indicates the obtained nanostructures with regular diffraction dots.

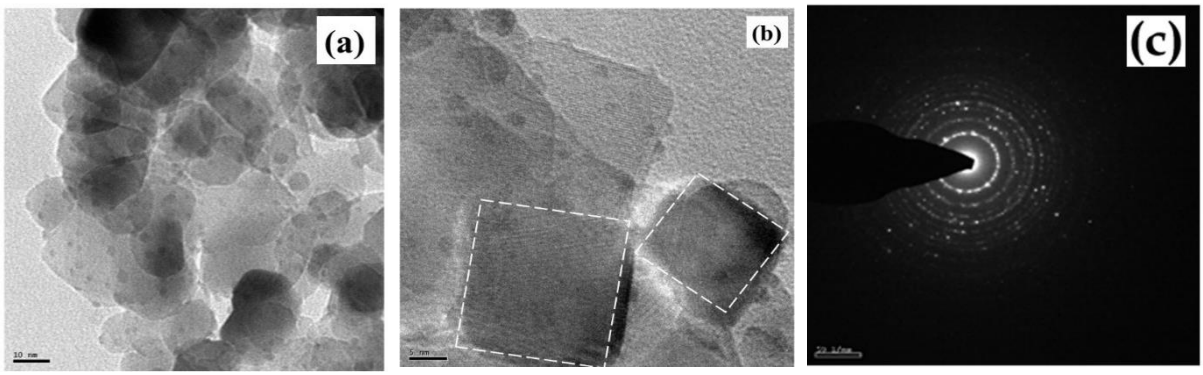

Figure 3. HR-TEM images of the $NiMn_2O_4$ nanostructures

3.4. Electrochemical Properties

3.4.1. Cyclic Voltammetry analysis

Figure 4 shows the cyclic voltammetry curves observed in 2 M KOH aqueous electrolyte in the potential window from 0.0 to 0.8 V at various applied scan rates between 5 and 100 mVs^{-1}. The symmetry of CV curves exhibits a rectangular shape, which reveals that the $NiMn_2O_4$ electrode indicates that fast charging-discharging characteristics and Non-faradic (double-layer capacitance) behavior. There are no redox peaks observed, indicating that the $NiMn_2O_4$ electrode prepared by the present method is charged and discharged at a pseudoconstant rate over the complete voltammetric cycle [19]. The specific capacitance (Sc) was calculated using the formula,

$$S_c = \frac{1}{v \times m(V_a - V_c)} \int_{V_a}^{V_c} IV \, \mathrm{dV} \qquad (2)$$

where, $\int_{V_a}^{V_c} IV \, \mathrm{dV}$ is the integral value during discharge, ***m*** is the mass of the electrode material loaded, v is the applied scan rate, and $(V_a - V_c)$ is the working potential window

[20]. The specific capacitance of $NiMn_2O_4$ was decreased, when the scan rate was increased between 5 mV/s and 100 mV/s. The specific capacitance decreases with the increase in the scan rates, signifying that the $NiMn_2O_4$ exhibit the high reversibility and reaction activity. Table 1 shows that the obtained specific capacitance of $NiMn_2O_4$ is higher than the earlier studied.

Table 1. Shows the comparison of obtained specific capacitance of $NiMn_2O_4$ with previously studied other materials

Material	Method	Specific capacitance (F/g)	Discharge Regime	Reference
$NiMn_2O_4$	Hydrothermal	370.5	1 A/g	[8]
$NiMn_2O_4$	In- situ	380	5mV/s	[21]
Sr-Cu oxide	Solid-state chemical reaction	308	4mA	[22]
Mn-Co Oxide	Ball milling	422	5mV/s	[23]
$NiMnO_3$/C	Co-precipitation	285	1 A/g	[24]
$NiMn_2O_4$	Hydrothermal-double hydroxide medium	854.7	5mV/s	Present work

The probable charge storage mechanism may be explained as

$$(NiMn_2O_4)_{surface} + K^+ + e^- = [KNiMn_2O_4]_{surface} \quad (4)$$

$$NiMn_2O_4 + K^+ + e^- - = [NiMn_2O_4]\ K \quad (5)$$

The potassium (K^+) ions are play a important role in supercapacitors. The de-intercalation and intercalation of K^+ ions in electrodes will result in the oxidation and reduction reactions in supercapacitors.

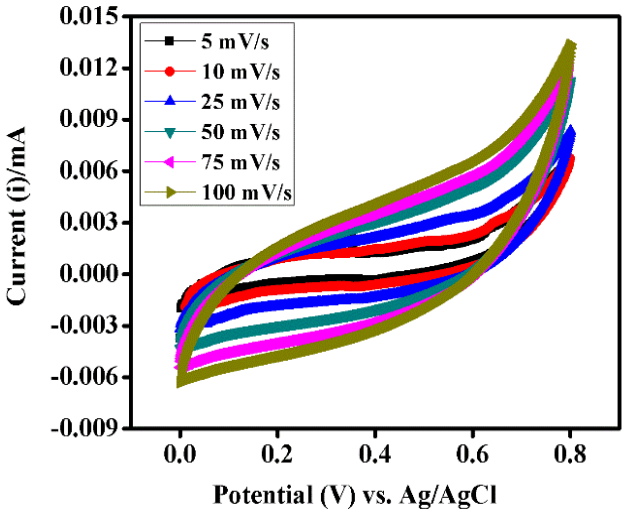

Figure 4. CV curves of the $NiMn_2O_4$ at various scan rates

The penetrating distance for K^+ ions in the electrodes is decreased with an increase in the scan rate. Once the applied scan rate is increased, the K^+ ions could only reach the outer surface of the electrodes. The specific capacitance will be reduced, when the interior part of $NiMn_2O_4$ could not participate in the reaction [25].

3.4.2. Charge-discharge analysis

The charge-discharge curves were recorded from 0.0 to 0.6 V at different current densities as shown in Fig. 5 (a). The obtained CP curves are good agreement with the CV analysis, which indicate the non-faradaic (double layer capacitor) behavior with very low current densities. The symmetric charge curves are corresponding to the discharge curves. From the CP curves, the increasing current density with decrease of charging/discharging time can be clearly observed, which explains the ion diffusion mechanism. A large active site of the electrode is employed by K^+ ions from electrolyte solution at lower current densities, offering higher specific capacitance. On the other hand, at higher current densities, inside the electrode material there is a limited accessibility of the K^+ ions, which results in the lower specific capacitance [26,27]. Furthermore, the specific capacitances are calculated using following formula,

$$C_s = \frac{I*t_d}{m*\nabla V} \qquad (3)$$

where, I - applied current, t_d – is the discharging time, m - is the mass of the material loaded, ∇V is the potential window difference (0.6 V). Cycling life is another important measurement for supercapacitor applications. Figure 5(b) shows the long cyclic stability of the $NiMn_2O_4$ electrode was studied up to 1000 cycles at 4 A/g.

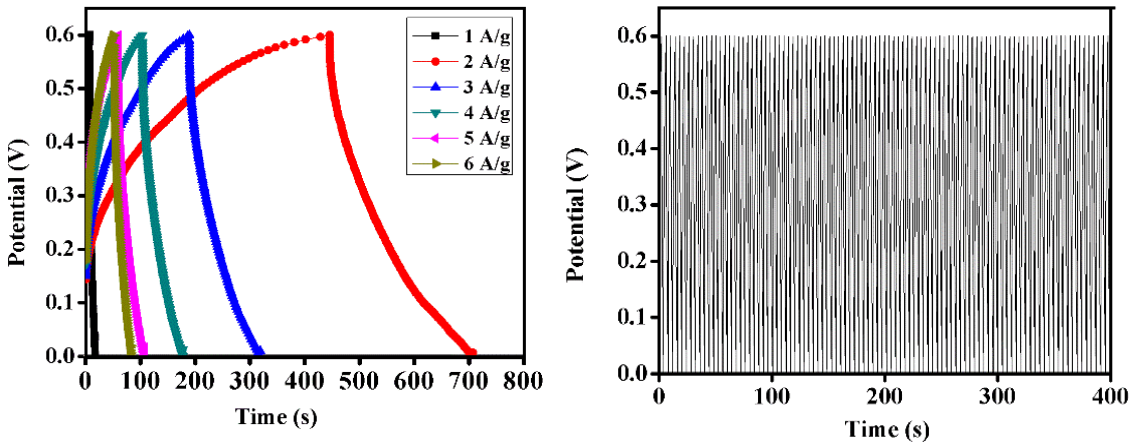

Figure 5. (a) CP curves of the $NiMn_2O_4$ at various current densities and (b) continuous long charge-discharge cycle at 4 Ag^{-1}

By using the following relation, the Columbic efficiency of the $NiMn_2O_4$ electrode is calculated,

$$\eta = (t_d / t_c) * 100 \qquad (4)$$

where, η is the columbic efficiency, t_c and t_d are the charging time and discharge time. The $NiMn_2O_4$ electrode revealed greater cycle efficiency about 94.6% over 10,00 cycles, demonstrating the oxides of both Ni and Mn elements are play vital roles for the enhancement of electrochemical properties of the electrode.

3.4.3. Electrochemical impedance spectroscopy analysis

Figure 6 shows the electrochemical impedance spectroscopy was analyzed in the frequency range between 1Hz and 1MHz. The Nyquist plot is can be classified into three parts; (i) high frequency region, (ii) middle frequency region and (iii) low frequency region. In the first part, the high frequency region revealed an approximate semicircle, non-zero intercept to the real axis gives the solution resistance (Rs). In the second part, the mid frequency region represents the charge transfer resistance (Rct). The values of 18 Ω and 55 Ω are observed for Rs and Rct from Nyquist plots, which show that the $NiMn_2O_4$ electrode has fast diffusion/transport and very low charge transfer resistance properties. In the third part, the low-frequency region the plot is linear line, which confirms much lower diffusion resistance of the electrolyte (OH^- ions) transport to the $NiMn_2O_4$ electrode during electrochemical reaction and good electrochemical reversibility [28].

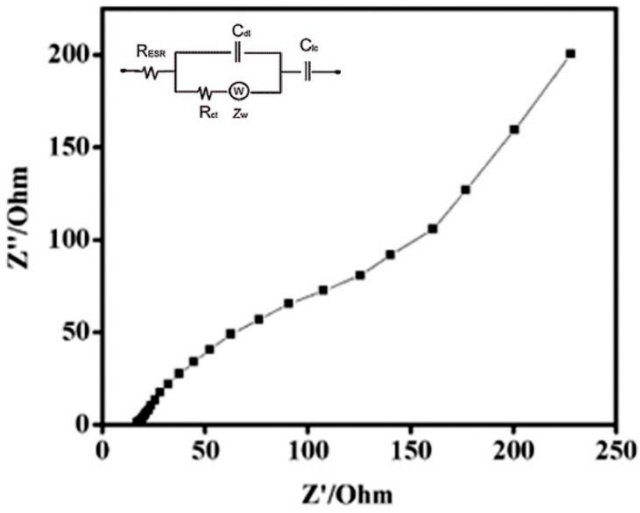

Figure 6. Electrochemical impedance spectroscopy of the $NiMn_2O_4$ electrode

3.4.4. Specific capacitance

Figure 7 shows the specific capacitances were calculated at various applied scan rates. The specific capacitance is mainly depended on the applied scan rate, i.e. The specific capacitance was increased to 854.7 Fg^{-1} at the lower scan rate of 5 mV/s, due to the $NiMn_2O_4$ could be utilized by the electrolyte ions within the more active sites and contributed to more charges to increase the specific capacitance. The specific capacitance was 312.4 Fg^{-1} at a high scan rate

of 100 mV/s. The $NiMn_2O_4$ electrode is delivered the highest specific capacitance than the previously studied materials. Variation of specific capacitance with different current densities as shown in inset Figure 7.

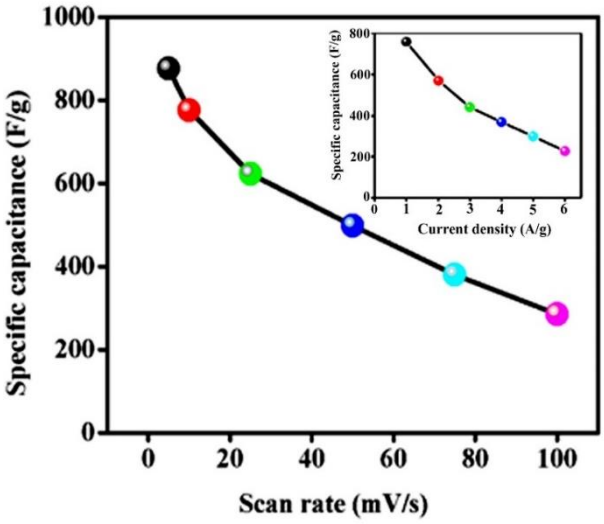

Figure 7. Specific capacitance vs scan rate and inset figure illustrates the SC value with different current densities

4. CONCLUSION

In summary, Cubic-like $NiMn_2O_4$ nanostructured material has been successfully synthesized by using KOH/NaOH double hydroxide medium through hydrothermal technique and further studied for high-performance supercapacitors. The specific capacitance was found to be 854.7 F/g in 2M KOH aqueous electrolyte at 5 mV/s. The $NiMn_2O_4$ electrode delivered the better cyclic stability (~94.6 % after 1000 cycles). The spinel structured $NiMn_2O_4$ electrodes possess very high specific capacitance and excellent cyclic stability. Compared with other materials, the $NiMn_2O_4$ is effective charge transfers and more ion diffusions, leading to the enhanced electrochemical properties. Due to enhanced electrochemical properties, $NiMn_2O_4$ electrode is very much suitable for future generation energy storage and conversion device applications.

Funding

This study was not funded

Conflict Of Interest

The authors declared that there is no conflicts of interest.

REFERENCES

[1] N. Shaheen, M. Aadil, S. Zulfiqar, H. Sabeeh, P.O. Agboola, M.F. Warsi, M.F. Aly Aboud, and I. Shakir, Ceram. Int. 4 (2021) 5273.

[2] H. Chen, X. Du, R. Wu, Y. Wang, J. Sun, Y. Zhang, and C. Xu, Nanoscale Adv. 2 (2020) 3263.

[3] M. Dinesh, Y. Haldorai, R. Thangavelu, and R. Kumar, Ceram Int. 46 (2020) 28006.

[4] J.H. Zheng, R.M. Zhang, P.F. Yu, and X.G. Wang, J. Alloys Compd. 772 (2019) 359.

[5] Y.X. Zhang, L. Su, B. Gao, and L. Shen, J. Mater. Chem. 19 (2009) 5772.

[6] V. Venkatachalam, A. Alsalme, A. Alswieleh, R. Jayavel. J. Mater. Sci. Mater. Electron. 29 (2018) 6059.

[7] S. He, and W. Chen, J. Power Sources 294 (2015) 150.

[8] H. Wei, J. Wang, L. Yu, Y. Zhang, D. Hou, and T. Li, Ceram Int. 42 (2016) 14963.

[9] V. Venkatachalam, A. Alsalme, A. Alghamdi, and R. Jayavel, Ionics 23 (2017) 977.

[10] D.H. Deng, H. Pang, J.M. Du, J.W. Deng, S.J. Li, J. Chen, and J.S. Zhang, Cryst. Res. Technol. 47 (2012) 1032.

[11] M. Puratchi Mani, K. Ponnarasi, A. Rajendran, V. Venkatachalam, K. Thamizharasan, and M. Jothibas, J. Elec. Mater. 49 (2020) 5964.

[12] L. Xiang, J. Shen, L. Lv, X. Li, S. Liu, and Z. Li, Key Eng. Mater. 727 (2018) 678.

[13] M.H.S. Ouaguenouni, A. Benadda, A. Kiennemann, A. Barama, and C. R. Chimie. 12 (2009) 740.

[14] Y. Gawli, S. Badadhe, A. Basu, D. Guin, M.V. Shelke, and S. Ogale, Sens. Actuators B 191 (2014) 837.

[15] H.M. Lee, K. Lee, and C.K. Kim, Materials 7 (2014) 265.

[16] M.Y. Arsent'ev, N.Y. Koval'ko, A.V. Shmigel', P.A. Tikhonov, and M. V. Kalinina, Glass. Phys. Chem. 43 (2017) 376.

[17] J. Zhang, Y. Sun, X. Li, and J. Xu, Sci. Rep. 9 (2019) 18121.

[18] A. Ray, A. Roy, M. Ghosh, J. Alberto, R. Ramón, S. Saha, U. Pal, S.K. Bhattacharya, and S. Das, Appl. Surf. Sci. 463 (2019) 513.

[19] L. Bao, J. Zang, and X. Li, Nano Lett. 11 (2011) 1215.

[20] V. Venkatachalam, and R.Jayavel, J. Electron. Mater. 49 (2020) 3174.

[21] P. Ahuja, S.K. Ujjain, R.K. Sharma, and G. Singh, RSC Adv. 4 (2014) 57192.

[22] H.R. Barai, Md. M Rahman, M. Roy, P. Barai, and S.W. Joo, Mater. Sci. Semicond. Process 90 (2019) 245.

[23] Z. Wang, J. Zhu, P.Sun, P. Zhang, Z. Zeng, S. Liang, and X. Zhu, J. Alloy Compd. 598 (2014) 166.

[24] A. Pendashteh, R.B. Kaner, A. Abbasi, M.F. Mousavi, M.F. El-Kady, M. Najafi, M.A. Kiani, M.S. Rahmanifar, M. Hashami, and P. Kakvand, Nanotechnology 27 (2016) 315401.

[25] C.H. Wu, J-S. Ma, and C.H. Lu, Curr. Appl. Phys. 12 (2012) 1190.
[26] M. Zhang, S. Guo, L. Zheng, G. Zhang, Z. Hao, L. Kang, Z.H. Liu, Electrochim. Acta 87 (2013) 546.
[27] U.J. Chavan, and A.A. Yadav, J. Mater. Sci. Mater. Electron. 28 (2017) 4958.
[28] Y. Sun, J. Zhang, X. Sun, and N. Huang, Cryst. Eng. Comm. 22 (2020) 1645.